Photoelectron Imaging of Doubly Charged Anions, $^{-}O_2C(CH_2)_nCO_2^{-}$ ($n = 2-8$): Observation of Near 0 eV Electrons Due to Secondary Dissociative Autodetachment

Xiao-Peng Xing,[†,‡] Xue-Bin Wang,[†,‡] and Lai-Sheng Wang*[,§]

Department of Physics, Washington State University, 2710 University Drive, Richland, Washington 99354, Chemical & Materials Sciences Division, Pacific Northwest National Laboratory, MS K8-88, Richland, Washington 99352, and Department of Chemistry, Brown University, Providence, Rhode Island 02912

Received: February 5, 2010; Revised Manuscript Received: March 5, 2010

The hallmark of multiply charged anions is the repulsive Coulomb barrier (RCB), which prevents low-energy electrons from being emitted in photodetachment experiments. However, using photoelectron imaging, we have observed persistent near 0 eV electrons during photodetachment of doubly charged dicarboxylate anions, $^{-}O_2C(CH_2)_nCO_2^{-}$ (D_n^{2-}, $n = 2-8$). Here we show that these low-energy electron signals are well structured and are independent of the detachment photon fluxes or energies. The relative intensities of these signals are dependent on n, with maxima at $n = 2$, 4, and 6. These near 0 eV electrons cannot come from direct photodetachment of the dianions and are proposed to come from decarboxylation of the product radical anions upon photodetachment of the parent dianions [$^{\bullet}O_2C(CH_2)_nCO_2^{-} \rightarrow CO_2 + {}^{\bullet}(CH_2)_nCO_2^{-}$], followed by dissociative autodetachment [$^{\bullet}(CH_2)_nCO_2^{-} \rightarrow (CH_2)_n + CO_2 + e$] or hydrogen-transfer-induced electron detachment [$^{\bullet}(CH_2)_nCO_2^{-} \rightarrow CH_2{=}CH(CH_2)_{n-2}CO_2H + e$]. Energetic considerations suggest that these processes are exothermic. It is further observed that solvation by one water molecule quenches the low-energy electron signals in the spectra of $D_n^{2-}(H_2O)$, consistent with the proposed mechanisms. These indirect dissociative autodetachment processes are expected to involve cyclic transition states for $n > 2$, which is in agreement with the dependence on the chain length due to the anticipated strains in the intermediate steps. The quenching of the low-energy electron signals by one water molecule demonstrates the importance of solvation on chemical reactions.

I. Introduction

Multiply charged anions (MCAs) are ubiquitous in solid states and liquid solutions. However, it was challenging to generate and investigate free MCAs in the gas phase due to the strong intramolecular Coulomb repulsion without the stabilization of counterions or solvation.[1] The electrospray ionization technique[2] has been shown to be an ideal method to transfer MCAs to the gas phase.[3] A major advance in the study of MCAs came from the coupling of electrospray with photoelectron spectroscopy (PES),[4,5] which has allowed a wide range of MCAs present in solutions to be investigated in the gas phase.[6,7] One of the most interesting physical properties of MCAs is the presence of the repulsive Coulomb barrier (RCB),[4] which derives from the short-range binding and long-range Coulomb repulsion between an electron and a negatively charged ion. The RCB provides dynamic stability to MCAs[8] and prevent low-energy electrons from being emitted, leading to a universal cutoff in the high binding energy side (low electron KEs) in PES of MCAs.[4−7] Therefore, ZEKE (zero electron kinetic energy) spectroscopy[9] cannot be applied to MCAs because tunneling probabilities through the RCB near threshold would be negligible.[10] The high binding energy cutoff has become a hallmark in PES of MCAs and provides a quantitative measure to the magnitude of the RCB.

A recent advance in the study of MCAs involves photoelectron imaging.[11−13] Photoelectron imaging[14−16] was an extension of the velocity mapping method originally developed to record spatial distributions of photodissociation products.[17] With the development of the velocity-map imaging technique,[18] photoelectron imaging has become a highly valuable technique over the past several years for the investigation of negative ions.[19−23] In addition to energetic information, the imaging technique provides photoelectron angular distributions that contain valuable information about the electron emission dynamics. Its high collecting efficiency for low-energy electrons has led to significantly improved energy resolution, comparable to ZEKE spectroscopy, using the slow electron velocity-map imaging mode.[24] The electron emission dynamics from MCAs are expected to be strongly influenced by the intramolecular Coulomb repulsion. Using photoelectron imaging, we have shown recently that electron emissions from MCAs follow the directions of the intramolecular Coulomb repulsion regardless of the orbital from which the electron is emitted.[11,13] This observation suggested that structural information can be obtained from photoelectron imaging of MCAs.[12]

Our first photoelectron imaging experiment was focused on a series of linear dicarboxylate dianions, $^{-}O_2C{-}(CH_2)_n{-}CO_2^{-}$ (D_n^{2-}) ($n = 3-8$).[11,13] In addition to the interesting angular distributions, we also observed strong near 0 eV electron signals, in particular, for small n. Because of the RCB, MCAs can be viewed as "anti-ZEKE" species, which cannot produce threshold or near 0 eV electrons. Therefore, the observation of the strong near 0 eV electron signals in the imaging experiment was puzzling. In this article, we explore the origins of these low-energy electrons. Specifically, we extend our study to the smallest stable dicarboxylate dianion (D_2^{2-}), which exhibits the strongest near 0 eV electron signals. We find that these signals

* Corresponding author. E-mail: Lai-Sheng_Wang@brown.edu.
† Washington State University.
‡ Pacific Northwest National Laboratory.
§ Brown University.

10.1021/jp1011523
Published on Web 03/17/2010

are highly structured and independent of the photodetachment photon energies or fluxes. Most interestingly, we observe that solvation by one water molecule almost completely quenches these low-energy electrons in the photoelectron images of $D_n^{2-}(H_2O)$. These observations suggest that the low-energy electrons come from secondary effects of the primary photodetachment product, $^{\bullet}O_2C(CH_2)_nCO_2^-$, most likely via decarboxylation [$^{\bullet}O_2C(CH_2)_nCO_2^- \rightarrow CO_2 + {}^{\bullet}(CH_2)_nCO_2^-$], followed by dissociative or isomerization-induced autodetachment of the radical anion, $^{\bullet}(CH_2)_nCO_2^-$.

II. Experimental Method

The experiment was carried out on our electrospray PES apparatus[5] by replacing the original magnetic-bottle photoelectron analyzer with a velocity-map imaging system, details of which have been described recently.[13] In brief, the dicarboxylate dianions were produced via electrospray of the respective salt solutions at 1 mM concentration in a mixed water−methanol solvent. Anions exiting the electrospray source were directed into a room-temperature ion trap by a RF-only quadruple ion guide. Ions were pulsed out of the trap at 10 Hz repetition rate into the extraction zone of a time-of-flight mass spectrometer. Both the bare dicarboxylate dianions and those solvated with one or more water molecules could be observed readily. The dianions of interest were selected by the time-of-flight mass spectrometer and directed to the center of the photoelectron imaging system, where they were detached by a linearly polarized laser beam from a Nd/YAG laser at three wavelengths: 266, 355, and 532 nm. Typical fluxes of the laser beams were 1 mJ/cm^2 for 266 nm, 4.5 mJ/cm^2 for 355 nm, and 20 mJ/cm^2 for 532 nm. The nascent electron cloud was accelerated by a high voltage pulse applied to the imaging electrodes and was projected onto a phosphor screen behind a set of microchannel plates. The positions of the photoelectrons on the phosphor screen were recorded by a charge-coupled-device (CCD) camera and accumulated as a photoelectron image. The usual accumulation time was $\sim 10^5$ laser shots at a 10 Hz repetition rate.

Because the laser polarization was parallel to the surface of the microchannel plates and the phosphor screen detector, the original shape of the 3D electron clouds could be rebuilt through inverse Abel transformation from the recorded 2D images, which were performed using the BASEX program.[25] The electron binding energy spectra and photoelectron angular distributions were obtained from the rebuilt 3D images. The electron kinetic energy (KE) resolution (ΔKE/KE) of our imaging system is ~2.5% for electrons around 1 eV, as calibrated from the 266 and 355 nm spectra of Br^- and I^-.[13] This energy resolution is comparable to our previous magnetic-bottle apparatus.[5] However, the imaging method can achieve much better energy resolution for slow electrons.[24] The best resolved features in our experiment for slow electrons can reach 3 meV (fwhm), as shown in Figure 1c.

III. Experimental Results

Photoelectron Imaging of $^-O_2C-(CH_2)_2-CO_2^-$. Because of the strong intramolecular Coulomb repulsion, many common MCAs are not stable in the gas phase, such as SO_4^{2-},[1e] which requires at least three water molecules to be stabilized.[26] The D_2^{2-} dianion is the smallest stable dicarboxylate dianion with an electron binding energy of 0 eV.[27,28] The PES spectra of D_2^{2-} and its hydrated clusters $D_2^{2-}(H_2O)_x$ were previously reported.[28] In the present study, we obtained its photoelectron images at three detachment photon energies, as shown in Figure 1a. The rings in each image represent photodetachment transitions, and

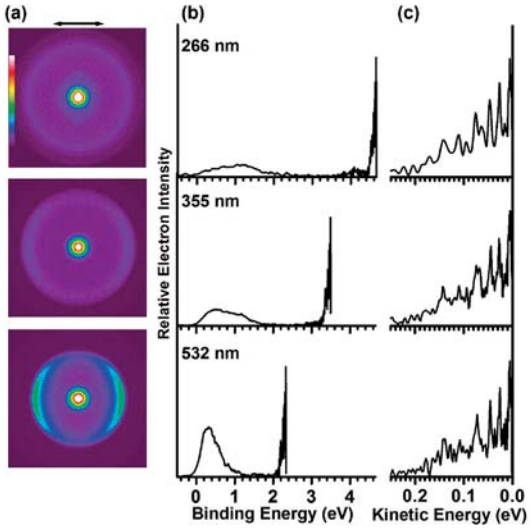

Figure 1. Photoelectron imaging of $^-O_2C(CH_2)_2CO_2^-$. (a) Symmetrized raw images at 266 (4.661 eV), 355 (3.496 eV), and 532 nm (2.331 eV) (from top to bottom). The double arrow indicates the directions of the laser polarization. The relative intensity scale bar is shown on the image at 266 nm. (b) Photoelectron spectra obtained from the images in part a. Photoelectron kinetic energies (KEs) were obtained from the radius (R) of the images after inverse Abel transformation, KE $\propto R^2$, calibrated by the photoelectron images of Br^- and I^-. The electron binding energies (BEs) were determined by BE = $h\nu$ − KE. The photoelectron intensities were obtained by integrating along all angles. (c) Enlarged view of the near 0 eV electron signals in part b, plotted in KE.

their diameters are proportional to the velocities of the outgoing photoelectrons. The decreasing radius of the outer ring from 266 to 532 nm shows the decreasing KEs of the photoelectrons. The ring changes from a nearly isotropic pattern at 266 nm to peaking in the direction parallel to the laser polarization at 355 and 532 nm. As previously reported,[11−13] the first detachment band of the D_n^{2-} dianions involved a perpendicular transition. However, the strong intramolecular Coulomb repulsion directs the outgoing electrons along the laser polarization, as shown more clearly in the 532 nm image of D_2^{2-}. As the electron KE increases, the effect of the intramolecular Coulomb repulsion decreases, resulting in the nearly isotropic distribution in the 266 nm image.[13] One dominating feature common to all three images in Figure 1a is the bright central spot, representing near 0 eV electrons. The sizes of these bright spots are identical for the three photon energies, and their shapes are isotropic.

After inverse Abel transformation, we obtained the PES spectra in electron binding energies, as shown in Figure 1b. The broad bands in the lower binding energy range, which correspond to the outer ring, are from direct photodetachment of D_2^{2-}. The onset near 0 eV binding energy is consistent with the prior PES data using the magnetic-bottle analyzer.[28] Furthermore, the low binding energy feature clearly shows a cutoff due to the RCB from 266 → 355 → 532 nm.

The high binding energy features in the PES spectra (Figure 1b) correspond to the bright central spot in the photoelectron images. These features are plotted in electron KEs in Figure 1c. Surprisingly, the features in all three detachment wavelengths are identical with well-resolved fine features. The fine features are quite sharp with peak widths on the order of a few millielectronvolts. The KEs of these features cover a range of 0 to 0.2 eV. Clearly, these features did not come from direct photodetachment of the parent D_2^{2-} dianion. The relative intensity of the low KE features is ~40% in the 266 and 355

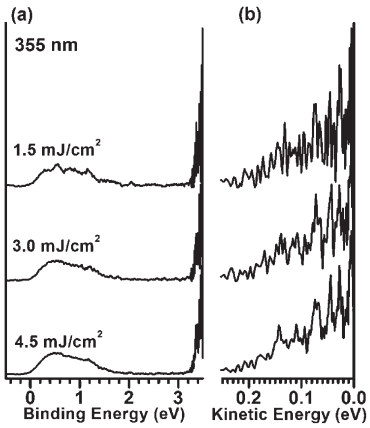

Figure 2. Photoelectron imaging of $^{-}O_2C(CH_2)_2CO_2^{-}$ at 355 nm and different laser fluxes. (a) Photoelectron spectra. (b) Enlarged view of the near 0 eV electron signals in the spectra of part a, plotted in KE.

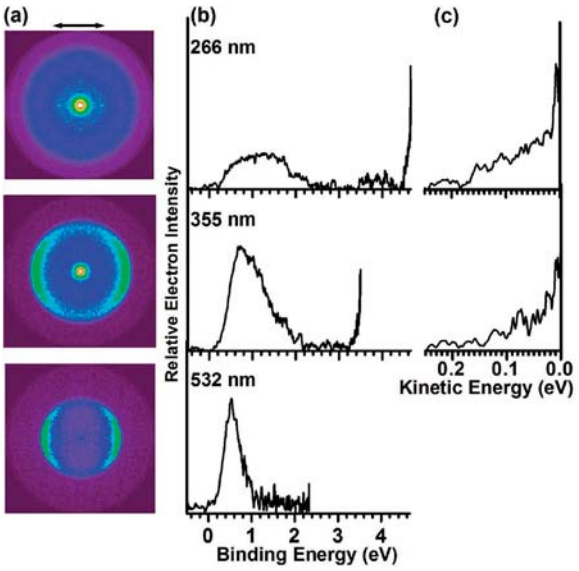

Figure 3. Photoelectron imaging of $^{-}O_2C(CH_2)_2CO_2^{-}(H_2O)$ at 266, 355, and 532 nm. (a) Symmetrized raw images. (The color scale is the same as that in Figure 1.) (b) Photoelectron spectra obtained from part a. (c) Enlarged view of the near 0 eV electron signals in part b, plotted in KE.

nm spectra and 20% in the 532 nm spectrum in comparison with the main detachment band at low binding energies, as measured by the integrated areas for the near 0 eV electrons between 0 and 0.23 eV over that of all direct photodetachment signals.

To test the possibility of multiphoton effects, we studied the dependence of these near 0 eV electrons on the detachment laser fluxes, as shown in Figure 2. We observed that the spectral pattern and the relative intensity of the slow electrons are identical for the three different photon fluxes, except that the signal-to-noise ratio decreased at lower photon fluxes, clearly showing that both fast and slow electrons are from single-photon processes.

Photoelectron Imaging of $D_2^{2-}(H_2O)$. To examine the effect of solvation on the near 0 eV electron signals, we obtained photoelectron images of $D_2^{2-}(H_2O)$, as shown in Figure 3a. The angular distributions and the trend with photon energies of the main feature in the images of $D_2^{2-}(H_2O)$ are similar to those of D_2^{2-} (Figure 1a). The central bright spot due to near 0 eV electrons were present in the 266 and 355 nm images but

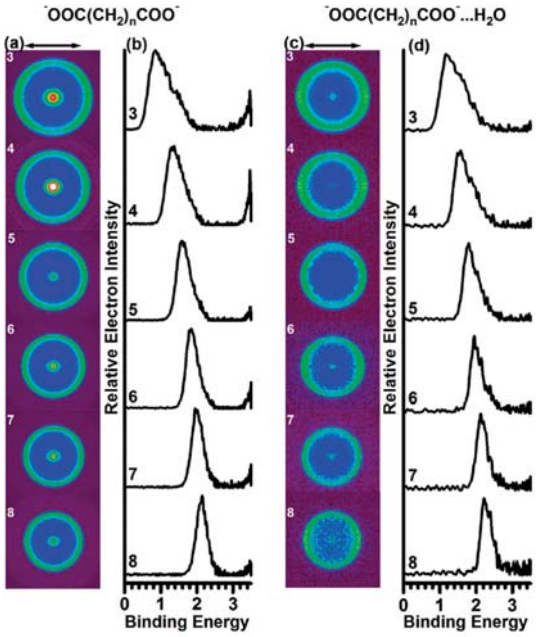

Figure 4. Photoelectron imaging of $^{-}O_2C(CH_2)_nCO_2^{-}$ and $^{-}O_2C(CH_2)_n$-$CO_2^{-}(H_2O)$ ($n = 3-8$) at 355 nm. (a,c) Symmetrized raw images of $^{-}O_2C(CH_2)_nCO_2^{-}$ (ref 11) and $^{-}O_2C(CH_2)_nCO_2^{-}(H_2O)$, respectively. (The color scale is the same as that in Figure 1.) (b,d) Photoelectron spectra obtained from the images in parts a and c, respectively.

disappeared in the 532 nm image. Figure 3b shows the PES spectra in electron binding energies. Because the mass intensity of the $D_2^{2-}(H_2O)$ dianion was much weaker than that of D_2^{2-}, the signal-to-noise ratios of the spectra in Figure 3b are lower than those in Figure 1b. The electron binding energies increased to ~0.3 eV in $D_2^{2-}(H_2O)$, consistent with the prior report using the magnetic-bottle apparatus.[28] The near 0 eV electron signals at 266 and 355 nm are displayed in electron KEs in Figure 3c. The energy range of these near 0 eV electrons is similar to that in the D_2^{2-} spectra (Figure 1c), that is, ~0.2 eV above 0 eV, but no fine features were resolved. The relative intensities as measured by the integrated areas of the slow electrons in the solvated species were significantly reduced, amounting to ~10% at 266 nm and 5% at 355 nm and becoming negligible at 532 nm.

Photoelectron Imaging of $D_n^{2-}(H_2O)$ in Comparison with that of D_n^{2-} ($n = 3-8$). Photoelectron images of D_n^{2-} ($n = 3-11$) at 355 and 266 nm have been reported previously, and near 0 eV signals were observed for all species.[11,13] To see how solvation influences these signals, we have taken photoelectron images for $D_n^{2-}(H_2O)$ ($n = 3-8$) at 355 nm to compare with those of the bare dianions (Figure 4). Figure 4a,b shows the symmetrized raw images and the converted PES spectra in binding energies of D_n^{2-} ($n = 3-8$) at 355 nm, respectively. These data have been previously reported in detail.[11] The bright central spot in these images were obvious, in particular, the relative intensities of the near 0 eV electrons appeared to be size-dependent with local maxima at $n = 4$ and 6.

Figure 4c,d shows the symmetrized raw images and the PES spectra in electron binding energies of $D_n^{2-}(H_2O)$ at 355 nm, respectively. The adiabatic electron binding energies of $D_n^{2-}(H_2O)$ shown in Figure 4d are ~0.2 to 0.3 eV higher than those of the corresponding D_n^{2-} in Figure 4b, which is consistent with those previously reported using the magnetic-bottle apparatus.[28-30] The anisotropy of the outer ring in the images of $D_n^{2-}(H_2O)$ is similar to that in D_n^{2-}. The most interesting observation was that there are no bright central spots in the

images of $D_n^{2-}(H_2O)$, and in the converted PES spectra (Figure 4d), there are no peaks in the high binding energy side.

IV. Discussion

Near 0 eV Electrons from D_n^{2-}: Evidence of Secondary Dissociative Autodetachment. Low-energy electron signals have been observed in PES of singly charged anions due to thermionic emissions in metal clusters,[31] fullerenes,[32] and even very small molecular anions.[33] In these cases, the parent anions absorb a photon via electronic excitation, which can rapidly relax via vibronic coupling to create a vibrationally hot anion, leading to thermionic emission.[34] Similar thermionic emission processes can be ruled out for the current D_n^{2-} dianions. First, the RCB would prohibit such processes. The low-energy electrons could only come from tunneling through the RCB, but the tunneling probabilities are negligible near threshold.[10] Second, the well-resolved fine features in the low-energy signals (Figure 1c) are inconsistent with thermionic emission processes, which produce electrons with continuous energy distributions.[34] Third, thermionic emission would be strongly dependent on the photon energies, in disagreement with our observations. Finally, the observed size dependence of the low-energy signals in D_n^{2-} is also inconsistent with the thermionic emission mechanism.

So, what is the origin of the near 0 eV electrons observed in the photodetachment of the D_n^{2-} dianions? Because of the RCB, the near 0 eV electron signals cannot be due to direct detachment from the parent dianions. The linear dependence on photon fluxes (Figure 2) indicates that these signals are not from multiphoton processes either. The similarity of these signals at different detachment laser wavelengths, as shown in Figure 1c, provides the most important clue, suggesting that they are most likely from secondary effects from the primary photodetachment product, $^{\bullet}O_2C-(CH_2)_n-CO_2^-$ ($D_n^{\bullet-}$). The interaction zone in our imaging system is ~5 mm around the center of the imaging lens assembly, and the daughter anions stay for ~100−200 ns in this region.[13] Therefore, any secondary processes of the daughter radical anion ($D_n^{\bullet-}$) taking place within this time window can be detected.

One possibility is autodetachment of the daughter radical anion: $D_n^{\bullet-} \rightarrow D_n + e$, initiated by excess energies left after direct photodetachment. The $D_n^{\bullet-}$ daughter anions generated in the primary photodetachment of D_n^{2-} could be in their ground states or different excited vibronic states. In the spectra shown in Figures 1 and 4, the threshold of the main detachment band corresponds to the ground state of $D_n^{\bullet-}$ and any features above the threshold correspond to either vibrational or electronic excited states of $D_n^{\bullet-}$. The width of the main detachment band represents the range of excitation energies in the $D_n^{\bullet-}$ daughter anions. For example, in Figure 1b, the maximum excitation energies in $D_2^{\bullet-}$ could be ~2, ~1.7, and ~1 eV at 266, 355, and 532 nm, respectively, which decrease with decreasing detachment photon energies. If the vibronic excitation energy is higher than the electron binding energy of the daughter anion $D_n^{\bullet-}$, autodetachment could occur. The adiabatic electron binding energies of $R-CO_2^-$ monocarboxylate anions were known to be ~3.2 eV[4,35−38] and were found to slightly depend on the alkyl groups. The electron binding energies of the radical anions $D_n^{\bullet-}$ are expected to be similar around 3.2 eV. However, the maximum available vibronic excitation energies even at 266 nm are far below the expected electron binding energies for $D_n^{\bullet-}$, ruling out the direct autodetachment channel, $D_n^{\bullet-} \rightarrow D_n + e$.

Alternatively, indirect autodetachment of $D_n^{\bullet-}$ can take place via dissociative detachment. We will show that such indirect dissociative detachment processes are energetically feasible by forming stable products and are likely responsible for the near 0 eV electrons. Furthermore and most importantly, Figure 1c shows that the spectra of the near 0 eV electrons are independent of the primary detachment photon energies. For D_n^{2-} ($n = 3-8$), we have also found that the spectra in the low KE range are quite similar at different photon energies. Because different photon energies produced different distributions of internal energies in the $D_n^{\bullet-}$ daughter anions, the above observations strongly suggest that the dissociative autodetachment involves multiple steps, where the initial energy distributions in $D_n^{\bullet-}$ have little effect on the KE distributions of the electrons emitted in the final autodetachment step.

Decarboxylation of the $^{\bullet}O_2C-(CH_2)_n-CO_2^-$ Radical Daughter Anions. In the gas phase, the monocarboxylate anions, $R-CO_2^-$, are stable with very high electron binding energies.[4,35−38] However, upon electron detachment, the $R-CO_2^{\bullet}$ radicals are unstable against decarboxylation because of the high stability of the CO_2 molecule. The simplest members of these species, that is, R = H and CH_3, have been extensively studied.[36,39,40] The decomposition rate constant of the acetyloxyl radical ($CH_3CO_2^{\bullet}$) was measured to be 1.6×10^9 s^{-1},[40b] corresponding to a lifetime of 0.6 ns. The decarboxylation exothermicity for $CH_3CO_2^{\bullet}$ is 17 ± 5 kcal/mol (~0.74 eV) with an activation energy of 6.6 kcal/mol (~0.29 eV)[40b] and that of $HCO_2^{\bullet}$ is known to be 0.58 ± 0.13 eV.[35] The dissociative dynamics of both $HCO_2^{\bullet}$ and $CH_3CO_2^{\bullet}$ have been studied using photoelectron−photofragment coincidence spectroscopy.[36,39] Upon photodetachment of $CH_3CO_2^-$ at 355 nm, 90% of the $CH_3CO_2^{\bullet}$ radicals were found to dissociate to $CH_3^{\bullet} + CO_2$. Analogously, the $^{\bullet}O_2C-(CH_2)_n-CO_2^-$ radical anions produced from photodetachment of the D_n^{2-} dianions are expected to undergo decarboxylation within nanosecond time scales

$$^{\bullet}O_2C-(CH_2)_n-CO_2^- \rightarrow {}^{\bullet}(CH_2)_n-CO_2^- + CO_2 \quad (1)$$

The decarboxylation exothermicity of channel 1 is expected to be similar to or larger than that of $CH_3CO_2^{\bullet}$. This energy and the original internal energies in $D_n^{\bullet-}$ are partitioned between the internal and KEs of the two fragments. However, the decarboxylation step of channel 1 does not produce an electron. Therefore, the $^{\bullet}(CH_2)_n-CO_2^-$ daughter anion must undergo further dissociative autodetachment to produce the near 0 eV electrons.

Proposed Mechanisms for the Indirect Dissociative Autodetachment of $^{\bullet}CH_2-CH_2-CO_2^-$. For $n = 2$, the first decarboxylation step generates a secondary radical anion, $^{\bullet}CH_2-CH_2-CO_2^-$, which can undergo further decarboxylation autodetachment (channel 2) or isomerization-induced autodetachment (channel 3) to produce stable molecular products and a free electron

$$^{\bullet}(CH_2)_2-CO_2^- \rightarrow CH_2{=}CH_2 + CO_2 + e \quad (2)$$

$$\rightarrow CH_2{=}CH-CO_2H + e \quad (3)$$

The energetics of channels 2 and 3 can be estimated using the known bond energies. The electron binding energy of $^{\bullet}(CH_2)_2-CO_2^-$ is expected to be similar to that for $CH_3CO_2^-$, which is 3.25 eV,[38] whereas the decarboxylation exothermicity of the diradical $^{\bullet}(CH_2)_2-CO_2^{\bullet}$ ($\rightarrow {}^{\bullet}CH_2CH_2^{\bullet} + CO_2$) is expected to be similar to $CH_3-CO_2^{\bullet}$, that is, ~0.74 eV. For channel 2, the formation of a double bond in $CH_2{=}CH_2$ gains about 2.74

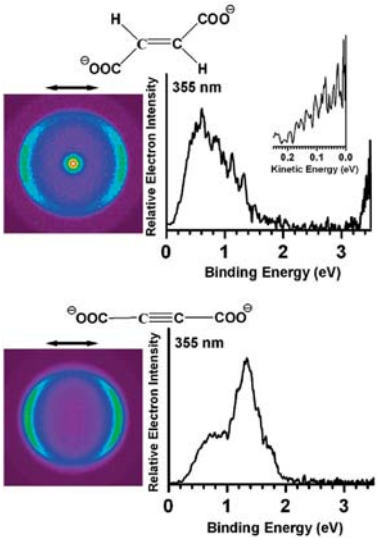

Figure 5. Photoelectron imaging of trans $^{-}O_2C-CH=CH-CO_2^{-}$ and $^{-}O_2C-C\equiv C-CO_2^{-}$ at 355 nm (left) and photoelectron spectra obtained from the images (right). The enlarged view of the near 0 eV electron signals in $^{-}O_2C-CH=CH-CO_2^{-}$ is plotted in electron kinetic energy.

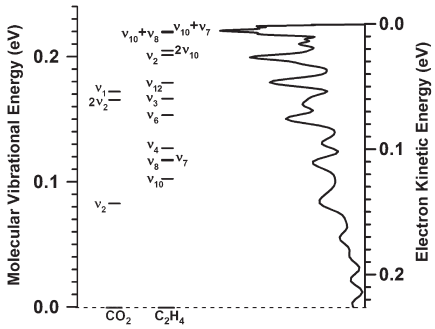

Figure 6. Comparison of the resolved fine features for the near 0 eV electron signals in photodetachment of $^{-}O_2C(CH_2)_2CO_2^{-}$ and the vibrational energy levels for CO_2 and C_2H_4.[42] The ground vibrational levels are aligned roughly with the maximum measured electron kinetic energies.

eV energy (the bond energy difference between a C=C double bond and a C−C single bond).[41] Therefore, the decarboxylation exothermicity (0.74 eV) and the bond energy gain (2.74 eV) add up to ∼3.48 eV, which exceeds the anticipated electron binding energy of $^{\bullet}(CH_2)_2-CO_2^{-}$ and yields an exothermicity of ∼0.2 eV for channel 2. Therefore, channel 2 is energetically possible even if the $^{\bullet}(CH_2)_2-CO_2^{-}$ radical anion contains no internal energies. Channel 3 involves an H atom transfer from the α-C to the $-CO_2^{\bullet}$ radical (breaking a C−H bond and forming an O−H bond) and the simultaneous formation of a C=C double bond. The O−H bond is stronger than the C−H bond by ∼0.53 eV.[41] This energy gain plus the energy gain in the formation of the C=C double bond gives an energy of ∼3.27 eV, which is similar to the expected electron binding energy of the $^{\bullet}(CH_2)_2-CO_2^{-}$ radical anion. Therefore, channel 3 is thermally neutral and should also be feasible, in particular, for $^{\bullet}(CH_2)_2-CO_2^{-}$ containing internal energies. Nevertheless, we expect that channel 2 should be dominant and will focus our discussion on this secondary dissociative autodetachment channel.

Further Evidence of the Proposed Indirect Dissociative Autodetachment Mechanisms. The feasibility of the proposed mechanism and the exothermicity of channel 2 depend on the formation of a new C−C bond. We have carried out two control experiments (Figure 5) on ethylene dicarboxylate ($^{-}O_2C-CH=CH-CO_2^{-}$) and acetylene dicarboxylate ($^{-}O_2C-C\equiv C-CO_2^{-}$), which provide direct support for our proposed mechanism for the production of the near 0 eV electrons. Decarboxylation of the primary detachment products, $^{\bullet}O_2C-CH=CH-CO_2^{-}$ and $^{\bullet}O_2C-C\equiv C-CO_2^{-}$, is expected to be similar for the two species, resulting in $^{\bullet}CH=CH-CO_2^{-}$ and $^{\bullet}C\equiv C-CO_2^{-}$ radical anions, respectively. However, the energetic of the second dissociative detachment step would be expected to be very different for the two systems. In the case of ethylene dicarboxylate, the final products are: $^{\bullet}CH=CH-CO_2^{-} \rightarrow CH\equiv CH + CO_2 + e$. The exothermicity of this process is expected to be similar to that of channel 2, and it is energetically feasible. Indeed, near 0 eV electron signals are observed, as shown in Figure 5 (top). In the case of acetylene dicarboxylate, the second step produces: $^{\bullet}C\equiv C-CO_2^{-} \rightarrow {}^{\bullet}C\equiv C^{\bullet} + CO_2 + e$. No new C−C bond can be formed in the C_2 fragment, and this channel is not expected to be feasible energetically. This conjecture is confirmed vividly in the photoelectron image (Figure 5, bottom), where no near 0 eV electrons are observed for acetylene dicarboxylate. These observations provide the most direct support for the two-step dissociative detachment processes represented by eqs 1 and 2.

Interpretation of the Well-Resolved Near 0 eV Electron Signals. In channel 2, the exothermicity and the initial internal energies of $^{\bullet}(CH_2)_2-CO_2^{-}$ deposited from the primary detachment and decarboxylation processes are expected to be partitioned between the internal energies of CO_2 and $CH_2=CH_2$ and the KEs of the two molecular products and the free electron. Considering the possible initial energy distributions in $^{\bullet}(CH_2)_2-CO_2^{-}$, it is surprising that fine features are observed in the near 0 eV electron signals (Figure 1). It is even more puzzling that these fine features seem to be independent of the primary detachment photon energies. These observations may be understood by careful considerations of the possible mechanism of the second dissociative autodetachment process. The products of $CH_2=CH_2 + CO_2 + e$ only correspond to the asymptotic limit of the dissociative autodetachment process. Note that the extra electron is initially located on the carboxylate end. It is most likely liberated from the molecular frame when the $C-CO_2^{-}$ bond distance (the reaction coordinate) enlarges to reach a critical point (or transition state), where ethylene and CO_2 are partially formed, $[CH_2=CH_2\cdots\cdots CO_2^{-}]$. At this point, the $-CO_2$ group is no longer able to hold the extra electron due to the negative electron affinity of CO_2.[42] Therefore, the energy carried away by the freed electron should only be sensitive to the initial vibrational excitation in the $C-CO_2^{-}$ bond (i.e., the reaction coordinate). The internal energies in the other vibrational modes in $^{\bullet}(CH_2)_2-CO_2^{-}$ should be largely retained in the $[CH_2=CH_2\cdots\cdots CO_2]$ activated complex and do not contribute to the outgoing electron. This consideration also suggests that the final $CH_2=CH_2$ and CO_2 products are not expected to carry any substantial amounts of the reaction exothermicity in the form of KEs, which is in excellent agreement with the fact that the observed maximum KE of ∼0.2 eV for the electrons is almost in exact agreement with the estimated exothermicity of channel 2.

Therefore, the exothermicity of channel 2 is expected to be partitioned primarily between the electron KEs and vibrational excitations in the CO_2 and $CH_2=CH_2$ products. The latter should correspond to the fine features in the near 0 eV electron signals. Figure 6 shows a comparison of the combined vibrational levels[43] of CO_2 and $CH_2=CH_2$ with the near 0 eV electron signals from the photoelectron images of D_2^{2-} in Figure 1. Even though the maximum energy release from channel 2 or the initial

internal energy distribution of $^{\bullet}CH_2-CH_2-CO_2^-$ was not known exactly, Figure 6 shows some similarity between the vibrational levels of the two fragments and the observed fine features, providing considerable credence for the proposed origin of the low-energy electrons.

Proposed Mechanisms for the Indirect Dissociative Autodetachment of $^{\bullet}(CH_2)_n-CO_2^-$ ($n \geq 3$). The two dissociative autodetachment paths of $^{\bullet}CH_2-CH_2-CO_2^-$ can be extended to longer molecular chains. However, the decarboxylation of $^{\bullet}(CH_2)_n-CO_2^-$ can lead to two different products, that is, either a cycloalkane, c-$(CH_2)_n$ (channel 4), or an alkene, $CH_2{=}CH-(CH_2)_{n-3}-CH_3$ (channel 5)

$$^{\bullet}(CH_2)_n-CO_2^- \rightarrow c\text{-}(CH_2)_n + CO_2 + e \quad (4)$$

$$\rightarrow CH_2{=}CH-(CH_2)_{n-3}-CH_3 + CO_2 + e \quad (5)$$

$$\rightarrow CH_2{=}CH-(CH_2)_{n-2}-CO_2H + e \quad (6)$$

The energetics of channels 4 and 5 should be similar to that of channel 2, and they should be exothermic, whereas channel 6 should have similar energetics as channel 3. In both channels 5 and 6, an H atom transfer is accompanied with the autodetachment, whereas in channel 4, a folding of the aliphatic chain is necessary during the dissociative autodetachment. However, all of these three channels would require cyclic transition states. The observed chain length dependence of the near 0 eV electron signals (Figure S1 of the Supporting Information) is consistent with this conjecture because the strain energies in the cyclic transition states are expected to depend on the chain length. For $n = 2$, channel 2 does not require any cyclic transition state and the dissociation is expected to be facile. Consequently, the D_2^{2-} spectra exhibit the strongest near 0 eV electron signals. It is well known that the strain energy of hexane is the smallest among cycloalkanes,[44] which may explain why D_6^{2-} displays a local maximum in the near 0 eV electron signals (Figure S1 of the Supporting Information). For channel 6, the H atom transfer for $n = 4$ involves a low-strain six-membered ring transition structure, which is consistent with the local maximum at $n = 4$ in the near 0 eV electron signals (Figure S1 of the Supporting Information).

Quenching of the Near 0 eV Electron Signals by Solvation. The relative intensities of the near 0 eV electrons in the spectra of $D_2^{2-}(H_2O)$ in Figure 3 decreased significantly in the 266 or 355 nm spectra and disappeared completely in the 532 nm spectrum. For the species with $n > 2$, the near 0 eV electron signals were negligible in the spectra of $D_n^{2-}(H_2O)$. The solvation by one water molecule has a profound effect on the secondary dissociative autodetachment of the D_n^{2-} dianions.

In prior research on the hydration of D_n^{2-}, we found that the first water molecule in $D_2^{2-}(H_2O)$ only interacts with one end of the dianions,[28−30,45] breaking the degeneracy of the two carboxylate groups. The stabilization to the electron binding energies of the carboxylate group by one water can be as large as 0.7 eV, as we recently reported for $CH_3CO_2^-(H_2O)$.[46] The electron binding energies of $D_2^{2-}(H_2O)$ shown in Figure 4 are only about 0.2 to 0.3 eV higher relative to the respective bare D_2^{2-} dianions because the water molecule exerts only a small effect to the other end of the dicarboxylates. Upon electron detachment, two types of $D_2^{\bullet-}(H_2O)$ radical anions are produced as a result of detachment from the two different terminal carboxylate groups

$$^-O_2C-(CH_2)_n-CO_2^-(H_2O) \rightarrow {}^{\bullet}O_2C-(CH_2)_n-CO_2^-(H_2O) + e \quad (7)$$

$$\rightarrow {}^-O_2C-(CH_2)_n-CO_2^{\bullet}(H_2O) + e \quad (8)$$

In channel 7, the decarboxylation of the primary detachment product will not be affected by the water solvation. However, the decarboxylation product, $^{\bullet}(CH_2)_n-CO_2^-(H_2O)$, is expected to be stable and cannot undergo further dissociative autodetachment: the strong stabilization of the carboxylate anion by the water (~0.7 eV) would make it endothermic. For channel 8, the water molecule interacts with the $-CO_2^{\bullet}$ radical and is expected to increase the activation energy of the first decarboxylation step. Apparently, for $n = 2$ at 355 and 266 nm, there were sufficient vibronic excitations to allow some of the $^-O_2C-(CH_2)_2-CO_2^{\bullet}(H_2O)$ product to undergo decarboxylation/dehydration to form $^-O_2C-(CH_2)_2^{\bullet}$, which can go on to yield the near 0 eV electron signals observed in Figure 3. However, at 532 nm, there were not sufficient vibronic excitations in the primary detachment product to allow the first decarboxylation/dehydration step. Therefore, no near 0 eV electrons were observed. For $n > 2$, apparently even at 355 nm, the first decarboxylation/dehydration step was shut off for the product of channel 8, giving rise to negligible near 0 eV electron signals (Figure 4). The effect of solvation provides indirect support for our proposed mechanisms for the origins of the observed near 0 eV electrons in the photoelectron images of D_n^{2-}. It is well known that solvation plays a major role in chemical reactions in the condensed phase. Our current observation shows that solvation by even one water molecule can dramatically alter the outcome of a chemical reaction.

V. Conclusions

We reported observation of near 0 eV electrons in photoelectron imaging of a series of doubly charged anions, $^-O_2C(CH_2)_nCO_2^-$ ($n = 2-8$), despite the fact that the RCBs prevent low-energy electrons to be emitted from multiply charged anions. We investigated the origins of these unexpected low energy electron signals by performing photon energy and flux dependence studies and examining the effects of water solvation. It was observed that the near 0 eV electron signals are independent of the photon energies and linear-dependent on photon fluxes and can be quenched by the solvation by one water molecule. It is proposed that the 0 eV electrons came from secondary dissociative autodetachment of $^-O_2C-(CH_2)_n^{\bullet}$, which were produced from spontaneous decarboxylation of the primary photodetachment products, $^-O_2C-(CH_2)_n-CO_2^{\bullet}$. The dramatic effect of one water molecule is interesting and demonstrates the importance of solvation on chemical reactions. The $^-O_2C-(CH_2)_n-CO_2^{\bullet}$ radical anions are ideal systems for photoelectron−photofragment coincidence spectroscopy to elucidate the detailed dissociation dynamics.

Acknowledgment. We thank Prof. A. I. Boldyrev and Ms. A. P. Sergeeva for valuable discussions and the National Science Foundation (CHE-0749496) for the support of this work.

Supporting Information Available: The intensities of the near 0 eV electrons relative to the primary photodetachment band from the photoelectron images of $^-O_2C(CH_2)_nCO_2^-$ ($n = 2-8$). This material is available free of charge via the Internet at http://pubs.acs.org.

References and Notes

(1) (a) Schauer, S. N.; Williams, P.; Compton, R. N. *Phys. Rev. Lett.* **1990**, *65*, 625. (b) Boldyrev, A. I.; Simons, J. *J. Phys. Chem.* **1994**, *98*, 2298. (c) Kalcher, J.; Sax, A. F. *Chem. Rev.* **1994**, *94*, 2291. (d) Scheller, M. K.; Compton, R. N.; Cederbaum, L. S. *Science* **1995**, *270*, 1160. (e) Boldyrev, A. I.; Gutowski, M.; Simons, J. *Acc. Chem. Res.* **1996**, *29*, 497. (f) Freeman, G. R.; March, N. H. *J. Phys. Chem.* **1996**, *100*, 4331. (g) Dreuw, A.; Cederbaum, L. S. *Chem. Rev.* **2002**, *102*, 181.

(2) Fenn, J. B. *Angew. Chem., Int. Ed.* **2003**, *42*, 3871.

(3) (a) Lau, T. C.; Wang, J.; Siu, K. W. M.; Guevremont, R. *J. Chem. Soc., Chem. Commun.* **1994**, 1487. (b) Blades, A. T.; Kebarle, P. *J. Am. Chem. Soc.* **1994**, *116*, 10761.

(4) (a) Wang, X. B.; Ding, C. F.; Wang, L. S. *Phys. Rev. Lett.* **1998**, *81*, 3351. (b) Wang, L. S.; Ding, C. F.; Wang, X. B.; Nicholas, J. B. *Phys. Rev. Lett.* **1998**, *81*, 2667.

(5) Wang, L. S.; Ding, C. F.; Wang, X. B.; Barlow, S. E. *Rev. Sci. Instrum.* **1999**, *70*, 1957.

(6) (a) Wang, L. S.; Wang, X. B. *J. Phys. Chem. A* **2000**, *104*, 1978. (b) Wang, L. S. *Comments Mod. Phys., Part D* **2001**, *2*, 207. (c) Wang, X. B.; Yang, X.; Wang, L. S. *Int. Rev. Phys. Chem.* **2002**, *21*, 473. (d) Yang, X.; Wang, X. B.; Fu, Y. J.; Wang, L. S. Probing the Electronic Structure of Fe-S Clusters: Ubiquitous Electron Transfer Centers in Metalloproteins Using Anion Photoelectron Spectroscopy in the Gas Phase. In *Principles Mass Spectrometry Applied to Biomolecules*; Laskin, J., Lifshitz, C., Eds.; Wiley-Interscience: Hoboken, NJ, 2006; pp 63−117. (e) Waters, T.; Wang, X. B.; Wang, L. S. *Coord. Chem. Rev.* **2007**, *251*, 474. (f) Wang, X. B.; Wang, L. S. *Annu. Rev. Phys. Chem.* **2009**, *60*, 105.

(7) (a) Arnold, K.; Balaban, T. S.; Blom, M. N.; Ehrler, O. T.; Gilb, S.; Hampe, O.; Lier, J. E. v.; Weber, J. M.; Kappes, M. M. *J. Phys. Chem. A* **2003**, *107*, 794. (b) Ehrler, O. T.; Furche, F.; Weber, J. M.; Kappes, M. M. *J. Chem. Phys.* **2005**, *122*, 094321. (c) Wang, X. B.; Woo, H. K.; Yang, J.; Kappes, M. M.; Wang, L. S. *J. Phys. Chem. C* **2007**, *111*, 17684.

(8) (a) Wang, X. B.; Wang, L. S. *Nature* **1999**, *400*, 245. (b) Wang, X. B.; Wang, L. S. *Phys. Rev. Lett.* **1999**, *83*, 3402. (c) Wang, X. B.; Ferris, K.; Wang, L. S. *J. Phys. Chem. A* **2000**, *104*, 25. (d) Weis, P.; Hampe, O.; Gilb, S.; Kappes, M. M. *Chem. Phys. Lett.* **2000**, *321*, 426. (e) Ehrler, O. T.; Yang, J. P.; Sugiharto, Unterreiner, A. N.; Kappes, M. M. J. *Chem. Phys.* **2007**, *127*, 184301. (f) Yang, J.; Xing, X. P.; Wang, X. B.; Wang, L. S.; Sergeeva, A. P.; Boldyrev, A. I. *J. Chem. Phys.* **2008**, *128*, 091102.

(9) Muller-Dethlefs, K.; Schlag, E. W. *Angew. Chem., Int. Ed.* **1998**, *37*, 1346.

(10) Wang, X. B.; Ding, C. F.; Wang, L. S. *Chem. Phys. Lett.* **1999**, *307*, 391.

(11) Xing, X. P.; Wang, X. B.; Wang, L. S. *Phys. Rev. Lett.* **2008**, *101*, 083003.

(12) Xing, X. P.; Wang, X. B.; Wang, L. S. *J. Phys. Chem. A* **2009**, *113*, 945.

(13) Xing, X. P.; Wang, X. B.; Wang, L. S. *J. Chem. Phys.* **2009**, *130*, 074301.

(14) Helm, H.; Bjerre, N.; Dyer, D. J.; Huestis, D. L.; Saeed, M. *Phys. Rev. Lett.* **1993**, *70*, 3221.

(15) Pinare, J. C.; Baguenard, B.; Bordas, C.; Broyer, M. *Phys. Rev. Lett.* **1998**, *81*, 2225.

(16) Deyerl, H. J.; Alconcel, L. S.; Continetti, R. E. *J. Phys. Chem. A* **2001**, *105*, 552.

(17) Chandler, D. W.; Houston, P. L. *J. Chem. Phys.* **1987**, *87*, 1445.

(18) Eppink, A. T. J. B.; Parker, D. H. *Rev. Sci. Instrum.* **1997**, *68*, 3477.

(19) Surber, E.; Sanov, A. *J. Chem. Phys.* **2002**, *116*, 5921.

(20) Davis, A. V.; Wester, R.; Bragg, A. E.; Neumark, D. M. *J. Chem. Phys.* **2003**, *118*, 999.

(21) Rathbone, G. J.; Sanford, T.; Andrews, D.; Lineberger, W. C. *Chem. Phys. Lett.* **2005**, *401*, 570.

(22) Sobhy, M. A.; Castleman, A. W., Jr. *J. Chem. Phys.* **2007**, *126*, 154314.

(23) Mccunn, L. R.; Gardenier, G. H.; Guasco, T. L.; Elliott, B. M.; Bopp, J. C.; Relph, R. A.; Johnson, M. A. *J. Chem. Phys.* **2008**, *128*, 234311.

(24) Osterwalder, A. M.; Nee, J.; Zhou, J.; Neumark, D. M. *J. Chem. Phys.* **2004**, *121*, 6317.

(25) Dribinski, V.; Ossadtchi, A.; Mandelshtam, V. A.; Reisler, H. *Rev. Sci. Instrum.* **2002**, *73*, 2634.

(26) Wang, X. B.; Nicholas, J. B.; Wang, L. S. *J. Chem. Phys.* **2000**, *113*, 10837.

(27) Skurski, P.; Simons, J.; Wang, X. B.; Wang, L. S. *J. Am. Chem. Soc.* **2000**, *122*, 4499. (2000).

(28) (a) Minofar, B.; Mucha, M.; Jungwirth, P.; Yang, X.; Fu, Y. J.; Wang, X. B.; Wang, L. S. *J. Am. Chem. Soc.* **2004**, *126*, 11691. (b) Ding, C. F.; Wang, X. B.; Wang, L. S. *J. Phys. Chem. A* **1998**, *102*, 8633.

(29) Ding, C. F.; Wang, X. B.; Wang, L. S. *J. Phys. Chem.* **1998**, *102*, 8633.

(30) Yang, X.; Fu, Y. J.; Wang, X. B.; Slavicek, P.; Mucha, M.; Jungwirth, P.; Wang, L. S. *J. Am. Chem. Soc.* **2004**, *126*, 876.

(31) (a) Weidele, H.; Kreisle, D.; Recknagel, E.; Icking-Konert, G. S.; Handschuh, H.; Gantefor, G.; Eberhardt, W. *Chem. Phys. Lett.* **1995**, *237*, 425. (b) Gantefor, G.; Eberhardt, W.; Weidele, H.; Kreisle, D.; Recknagel, E. *Phys. Rev. Lett.* **1996**, *77*, 4524. (c) Pinare, J. C.; Baguenard, B.; Bordas, C.; Broyer, M. *Phys. Rev. Lett.* **1998**, *81*, 2225.

(32) (a) Wang, L. S.; Conceicao, J.; Jin, C.; Smalley, R. E. *Chem. Phys. Lett.* **1991**, *182*, 5. (b) Yeretzian, C.; Hansen, K.; Whetten, R. L. *Science* **1993**, *260*, 652. (c) Demirev, P.; Brinkmalm, G.; Eriksson, J.; Papaleo, R.; Hakansson, P.; Sundqvist, B. U. R. *Phys. Rev. B* **1994**, *50*, 9636. (d) Ding, D.; Compton, R. N.; Haufler, R. E.; Klots, C. E. *J. Phys. Chem.* **1993**, *97*, 2500.

(33) (a) Zhao, Y. X.; Beer, E.; Xu, C. S.; Taylor, T.; Neumark, D. M. *J. Chem. Phys.* **1996**, *105*, 4905. (b) Baguenard, B.; Pinaré, J. C.; Lépine, F.; Bordas, C.; Broyer, M. *Chem. Phys. Lett.* **2002**, *352*, 147. (c) Surber, E.; Sanov, A. *Phys. Rev. Lett.* **2003**, *90*, 093001.

(34) Klots, C. E. *J. Chem. Phys.* **1994**, *100*, 1035.

(35) Kim, E. H.; Bradforth, S. E.; Arnold, D. W.; Metz, R. B.; Neumark, D. M. *J. Chem. Phys.* **1995**, *103*, 7801.

(36) Lu, Z.; Continetti, R. E. *J. Phys. Chem. A* **2004**, *108*, 9962.

(37) Wang, X. B.; Woo, H. K.; Kiran, B.; Wang, L. S. *Angew. Chem., Int. Ed.* **2005**, *44*, 4968.

(38) Wang, X. B.; Woo, H. K.; Wang, L. S.; Minofar, B.; Jungwirth, P. *J. Phys. Chem. A* **2006**, *110*, 5047.

(39) Clements, T. G.; Continetti, R. E. *J. Chem. Phys.* **2001**, *115*, 5345.

(40) (a) Herk, L.; Feld, M.; Szwarc, M. *J. Am. Chem. Soc.* **1961**, *83*, 2998. (b) Braun, W.; Rajbenbach, L.; Eirich, F. R. *J. Phys. Chem.* **1962**, *66*, 1591. (c) Jaffe, L.; Prosen, E. J.; Szwarc, M. *J. Chem. Phys.* **1957**, *72*, 416. (d) Holmes, J. L.; Lossing, F. P.; Mayer, P. M. *J. Am. Chem. Soc.* **1991**, *113*, 9723.

(41) Stark, J. G.; Wallace, H. G. *Chemistry Data Book*; Murray: London, 1975.

(42) (a) Cooper, C. D.; Compton, R. N. *Chem. Phys. Lett.* **1972**, *14*, 29. (b) Compton, R. N.; Reinhardt, P. W.; Cooper, C. D. *J. Chem. Phys.* **1975**, *63*, 3821. (c) Klots, C. E.; Compton, R. N. *J. Chem. Phys.* **1978**, *69*, 1636.

(43) Shimanouchi, T. *Tables of Molecular Vibrational Frequencies. Consolidated Volume I*; National Bureau of Standards: Washington, DC, 1972.

(44) Chickos, J. S.; Hesse, D. G.; Panshin, S. Y.; Rogers, D. W.; Saunders, M.; Uffer, P. M.; Liebman, J. F. *J. Org. Chem.* **1992**, *57*, 1897.

(45) Wang, X. B.; Yang, J.; Wang, L. S. *J. Phys. Chem. A* **2008**, *112*, 172.

(46) Wang, X. B.; Jagoda-Cwiklik, B.; Chi, C. X.; Xing, X. P.; Zhou, M. F.; Jungwirth, P.; Wang, L. S. *Chem. Phys. Lett.* **2009**, *477*, 41.

JP1011523